Diffusion of Selective Penetrants in Interfacially Modified Block Copolymers from Molecular Dynamics Simulations

Youngmi Seo, Jonathan R. Brown, and Lisa M. Hall*

William G. Lowrie Department of Chemical and Biomolecular Engineering, The Ohio State University,
151 W. Woodruff Ave., Columbus, OH 43210

E-mail: hall.1004@osu.edu

ABSTRACT

To show the influence of the interface on structure and dynamics of microphase separated polymer systems, we study interfacially modified AB block copolymers with small molecule penetrants. The polymers have a random midblock or tapered midblock whose composition varies from pure A to pure B (or from pure B to pure A for an inverse taper) between two pure blocks of A and B. We perform simple coarse-grained molecular dynamics simulations of symmetric polymers that form lamellae. With normal tapering, both polymer and penetrant diffusion parallel to the lamellae increases as taper length increases. Inverse tapered polymers exist in different conformational states (e.g. stretched versus folded back and forth across the interface) with different dynamic behavior, leading to non-monotonic trends in their diffusion. However, the local mixing of monomers (rather than polymer conformation) appears to be the most important factor in determining penetrant diffusion.

Nanostructured block copolymers have been used as a transport medium in applications such as lithium ion batteries, fuel cells, and organic solar cells,[1–5] in which ions or polarizable molecules anisotropically diffuse through one microphase while the other provides mechanical strength. The interfaces of the microphase separated domains significantly affect transport; in one recent battery electrolyte example, Balsara and coworkers showed that conduction is hindered near interfaces.[6–9] Tapered AB block polymers (TBPs) have a size-tunable composition-gradient midblock. Thus, in addition to the overall fraction of A (f_A), Flory-Huggins interaction parameter (χ_{AB}), and chain length (N), there are two more crucial parameters: tapered midblock length (reported as a percentage or fraction, f_T, of chain length) and its composition. We consider a linear composition gradient, placed such that the A-rich side is connected to the A block (normal taper) or in reverse (inverse taper). With certain f_T, ion conduction can be increased even though tapering widens the interface.[10]

Tapering increases interfacial mixing, shortens domain spacing, decreases/widens the glass transition temperature (T_g), decreases the order-to-disorder transition temperature (T_{ODT}), and influences phase behavior and morphology.[11–26] Epps and coworkers showed that both normal and inverse tapers could form the bicontinuous double gyroid phase, which can be difficult to access in some diblock systems.[21] Self-consistent field theory (SCFT) work confirmed that normal tapering can widen the gyroid region of the phase diagram,[23] and that inverse TBPs can stitch/fold back and forth across the interface (related unique inverse TBP behavior had been illustrated experimentally).[18] Recent work on salt-doped TBP electrolytes showed normal (but not inverse) tapering enhanced conductivity.[10] Our previous MD studies examined normal TBPs and short inverse TBPs with and without sequence dispersity, reproducing the shorter lamellar spacing, wider interface, and easier access to a network phase expected, and showing effects of tapering on polymer diffusion and relaxation.[27,28] Sethuraman and Ganesan also studied TBPs via MD, including a mobility difference between monomer types, and showed the interfacial mixing and the mobility disparity have competing effects on the polymer dynamics.[29]

Here, we consider systems with added penetrants and systematically compare normal and inverse TBPs with random midblock systems as a function of f_T (or f_R for random midblock). We restrict our study to symmetric (f_A = 0.5) linear chains of N=40 in lamellae. We use a simple Kremer-Grest model nearly identical to our prior work (except including the attractive portion of the Lennard-Jones (LJ) interaction by changing the cutoff distance from $2^{1/6}\sigma$ to 2.5σ) with a wide range of $f_{T/R}$: 0, 0.3, 0.5, 0.6, 0.7, 1.0 for normal TBPs, 0.15, 0.3, 0.4, 0.5, 0.6, 0.7 for inverse TBPs, and 0.15, 0.3, 0.4, 0.5 for random midblocks (inverse TBPs at f_T=0.5 are unstable and discussed only in the Supporting Information). We initialize in lamellae following a procedure by Kremer and Grest,[30] except the less stable inverse TBPs with f_T = 0.4-0.85 were initialized based on fluids density functional theory (fDFT) results as described in our recent article (but also including penetrants).[26] Equal amounts of unbound penetrants C are initially distributed equally in the four A lamellae with a fixed bead number ratio [C]/[A] = 0.06. Within the taper or random midblock, each site is chosen to be A or B with a linearly varying (tapers) or 50% (random midblock) probability as in Ref. 27, leading to different sequences (see Figure 1). We note that others have compared different tapered/random compositions, including with nonlinear composition gradients and variable sequence blockiness.[15,31–33]

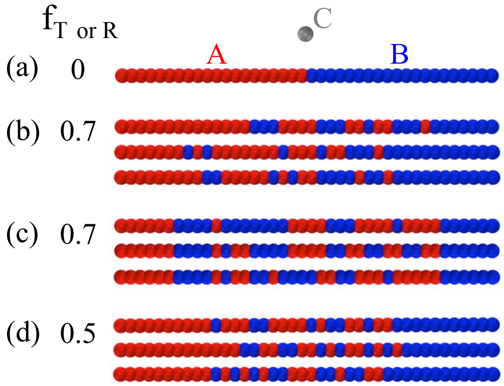

Figure 1. Example sequences for (a) diblock, (b/c) 70% normal/inverse tapers, and (d) 50% random midblock systems.

The segment-segment LJ interaction parameters (ϵ_{ij}) are chosen to cause phase separation and selective penetrant solvation; specifically, ϵ_{AB} = 0.43, ϵ_{BC} = 0.72, and ϵ_{AC} = 1.28. We make an analogy to how strongly lithium salts dissolve in the microphase with higher dielectric constant in the typical system of polystyrene-*b*-(polyethylene oxide); based on the discussion in Ref. 34 regarding Born solvation energy, and to match the previous work of Ref. 9 and 35, the difference in interaction strengths of C with A and B, i.e. $\Delta\chi = \chi_{BC} - \chi_{AC}$, of 8 is reasonable; the simple mapping as described in Ref. 30 which implies mapping to χ_{ij} using $\chi_{ij} \sim 14.07(1 - \epsilon_{ij}/\epsilon)$ yields this $\Delta\chi$ for our chosen interaction parameters. As a simple approach, we have chosen to drive this amount of selective solvation by applying the same size of both favorable A-C and unfavorable B-C interactions. The overall amount of selective solvation (difference in A-C and B-C interaction parameters) is also the same as the A-B segregation strength (note a relatively high A-B segregation strength is required for microphase separation of long inverse TBPs). We find similar results for two other choices of interaction strengths (see Supporting Information). While we are motivated by ion containing systems, the current model is a very generic and simple case of selective penetrants. The penetrants are not charged, however, we note that important advances are being made by many in efficiently and accurately including ionic effects in these and related systems, and charge-charge interactions can be crucial in understanding phase behavior and charge transport.[35–37] Figure 2 shows snapshots and density profiles for diblock and long normal and inverse tapered systems. The inverse tapered system shows an even wider interface and lower purity than the normal tapered system. The density profiles also clearly show that penetrants are concentrated in the A phase, i.e. the profile of penetrants generally follows that of A monomers, and they are somewhat more concentrated in the center of the A lamellae for the more segregated diblock system.

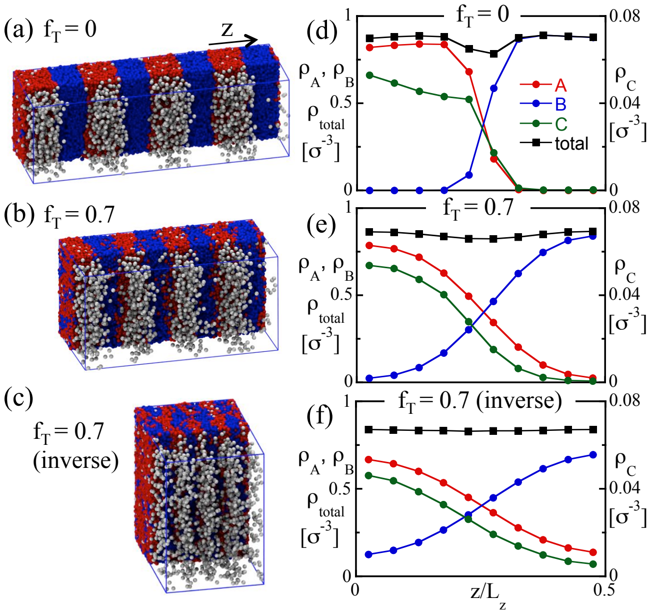

Figure 2. (a-c) Snapshots for $f_{T\ or\ T,inv}$ = 0 and 0.7 as labeled. A, B, and C beads are colored in red, blue, and gray, respectively. (d-f) Averaged number density profiles of the corresponding systems as labeled.

To better quantify the difference in interfacial A-B mixing among systems, we analyze the interfacial width relative to the lamellar spacing (see Figure 3a). The interfacial width (w) is obtained by fitting the profiles of $\rho_{A+C}(z)/\rho_{A+B+C}(z)$ to $\alpha + \beta \tanh\ (-2(z - z_0)/w)$ where α, β, and z_0 are adjustable parameters (see the Supporting Information). We also plot the number of A-B bonds per chain ($N_{A\text{-}B}$) averaged for all polymers. If the $N_{A\text{-}B}$ is large, the system is expected to have increased local interfacial A-B mixing. Figure 3b shows that for the three considered midblock systems, the value of averaged $N_{A\text{-}B}$ is generally in the order: random > inverse > normal; random midblocks statistically have more switches between monomer type along the chain.

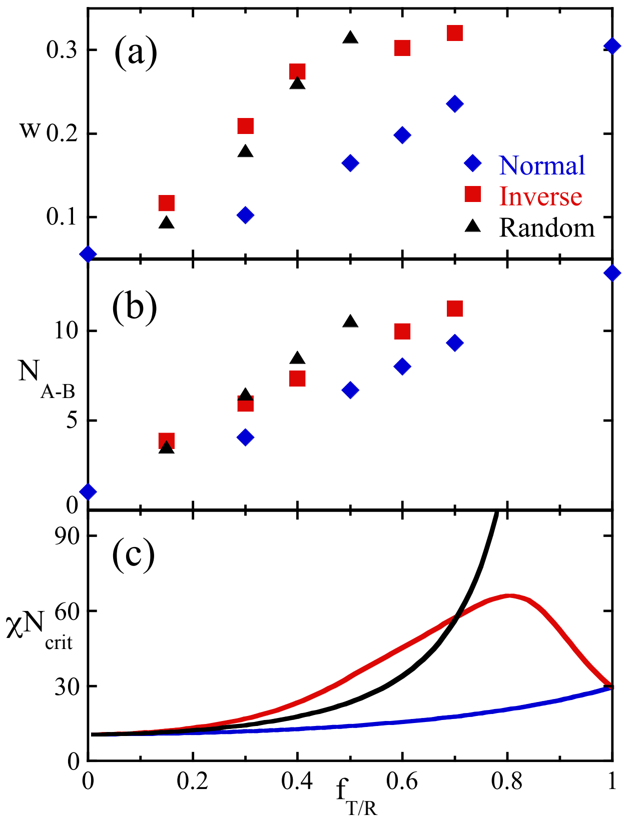

Figure 3. (a) Interfacial width (as a fraction of lamellar spacing), (b) averaged number of A-B bonds per chain, obtained from the simulated systems; these values are within ±0.08 of the statistically expected values, (c) critical χN from the RPA for normal and inverse TBPs and random midblocks as labeled. Note that the 50% inverse tapered system is not stable thus no points are reported for this system.

For context, we also provide in Figure 3c the critical χN values obtained using the random phase approximation (RPA) with the ideal tapered or random midblock composition profiles. This data is created in the same way as in Ref. 23, which also reported the tapered results but did not include random midblocks. Inverse tapers are slightly more miscible than random midblocks at low $f_{T/R}$ (both in terms of the critical χN where they microphase separate and the amount of mixing, as quantified by interfacial width, at constant χN). This indicates that the number of A-B bonds is not the only factor that determines the interfacial A-B mixing, because random midblocks have more A-B bonds than inverse tapers. Of course, as the taper or random midblock becomes the predominant part of the chain, the inverse and normal tapered systems both look like gradient copolymers (which still can form lamellae at a reasonable χN) while the random midblocks become increasingly difficult to phase separate.

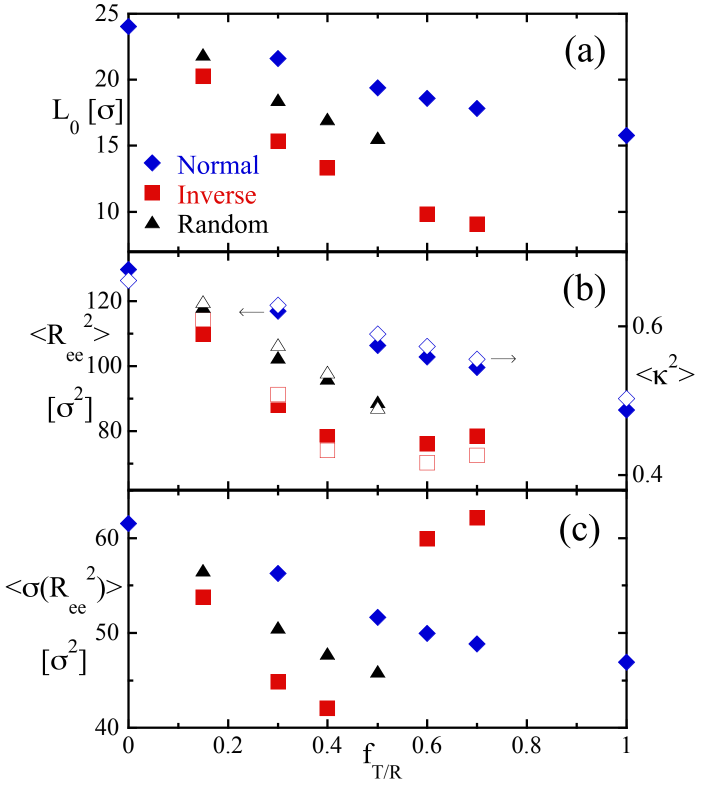

Figure 4. (a) Lamellar spacing, (b) polymers' mean-squared end-to-end distance (filled symbols) and shape anisotropy (empty symbols), and (c) standard deviation of the squared end-to-end distances, for normal and inverse tapered systems and random midblocks as labeled.

As is evident in prior work and in the snapshots of Figure 2, the lamellar spacing (L_0) significantly decreases for normal and inverse tapers versus diblocks. Figure 4a shows L_0 decreasing as $f_{T/R}$ increases, and that L_0 for normal tapers > L_0 for random midblocks > L_0 for inverse tapers. We expect that the L_0 of inverse TBPs would gradually increase for $f_T \geq 0.7$ to rejoin the normal TBPs' results at $f_T = 1$ (where normal and inverse tapers become identical). Figure 4b, c shows measures of chain size and conformation, specifically mean-squared end-to-end distance ($\langle R_{ee}^2 \rangle$) and its standard deviation among polymers ($\sigma(R_{ee}^2)$), and polymers' averaged shape anisotropy ($\langle \kappa^2 \rangle$). The shape anisotropy is obtained from the eigenvalues of the moment of inertia tensor, λ_1, λ_2, and λ_3 using the formula $\kappa^2 = 4 - 12(\lambda_1\lambda_2 + \lambda_1\lambda_3 + \lambda_2\lambda_3)/(\lambda_1 + \lambda_2 + \lambda_3)^2$, and ranges from 0 for spheres to 1 for straight rods.[38–40] All three of these properties monotonically decrease as a function of $f_{T/R}$ for normal TBPs and random midblocks as does their L_0. For inverse TBPs, these properties initially decrease then later increase after the taper or random midblock takes up more than about half of the chain. These non-monotonic structural behaviors of inverse TBPs and their relatively very short spacing compared to random midblocks (although the two systems have a relatively similar overall interfacial A-B mixing) are related to the inverse TBPs' unique and complex chain conformations.

We now can analyze in detail the inverse TBP conformational types possible across the entire range of inverse taper lengths. We classify chain conformations as folding, bridging, or stretching (across 1 or 2 layers), as shown by the examples at the top of Figure 5, by a simple algorithm based on the end-to-end distance and relative positions of the centers of mass (COM) of the chain's regions, A, B^t, A^t, and B, which refer to the pure A block, the following half of the taper block (majority B for an inverse taper), the other half of the taper block, and the pure B block, respectively. (The algorithmic details are given in the Supporting Information.) By visual inspection, we determined that this classification leads to polymers which appear similar to each other to be categorized together, and the examples shown in Figure 5 are representative of what polymers in these categories generally look like at intermediate taper lengths. To be able to categorize the diblocks and gradient copolymers analogously, we use a region near the middle/ends as the "taper" or "pure block"; specifically, we calculate as though $f_T = 0.1$ for diblocks and 0.9 for gradient copolymers.

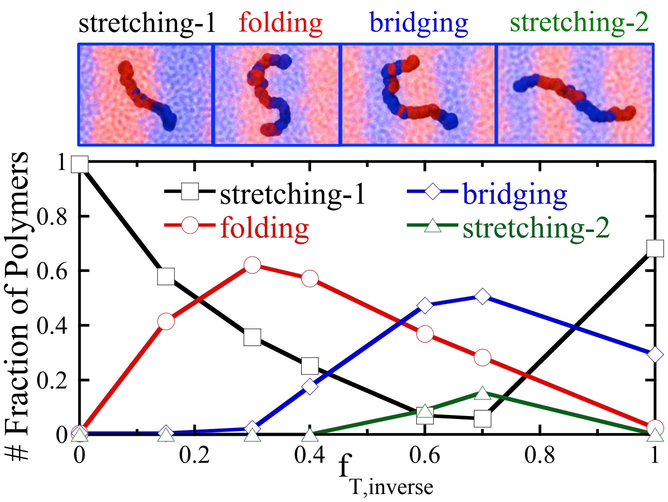

Figure 5. (Above) Snapshots of chain conformations for inverse TBPs; A and B monomers in red and blue, respectively, with all chains but one transparent in the background. The selected chain is smoothed by averaging each monomer's location over 21 snapshots each 115τ apart. The stretching-1 example has f_T = 0.3, others have f_T = 0.7. (Below) Fraction of polymers that show these conformations for inverse TBP systems.

We find that short inverse TBPs can only stretch across 1 layer or fold, but at $f_T > 0.3$, with longer tapers as well as the resulting shortened lamellar spacing, taper halves can cross the lamellae and bridging and stretching-2 conformations are seen. The bridging conformation is observed to be relatively unstable (more frequently switches to different conformations than the other conformational types do) until f_T = 0.6 – this was determined by roughly counting the number of contiguous snapshots in time for which polymers keep the bridging conformations (see the Supporting Information).

As f_T further increases, the chains can also fully stretch out; the fraction of stretching-2 conformations becomes noticeable at f_T = 0.6 and 0.7 where the $\langle R_{ee}^2 \rangle$ and $\langle \kappa^2 \rangle$ are increasing as a function of f_T though L_0 keeps decreasing, as intuitively expected from the nature of this conformation. For comparison, we applied the aforementioned procedure to determine chain conformations of normal tapers and random midblocks, and found that, for all considered $f_{T/R}$, more than 93% and 70% of polymers (respectively for normal tapers and random midblocks) have the typical "stretching-1" conformation. To briefly probe chain length effects, we simulated an analogous 40% inverse TBP system with twice longer chains (N =

80) at the same segregation strength; it showed very similar fractions of polymers by conformation (see the Supporting Information).

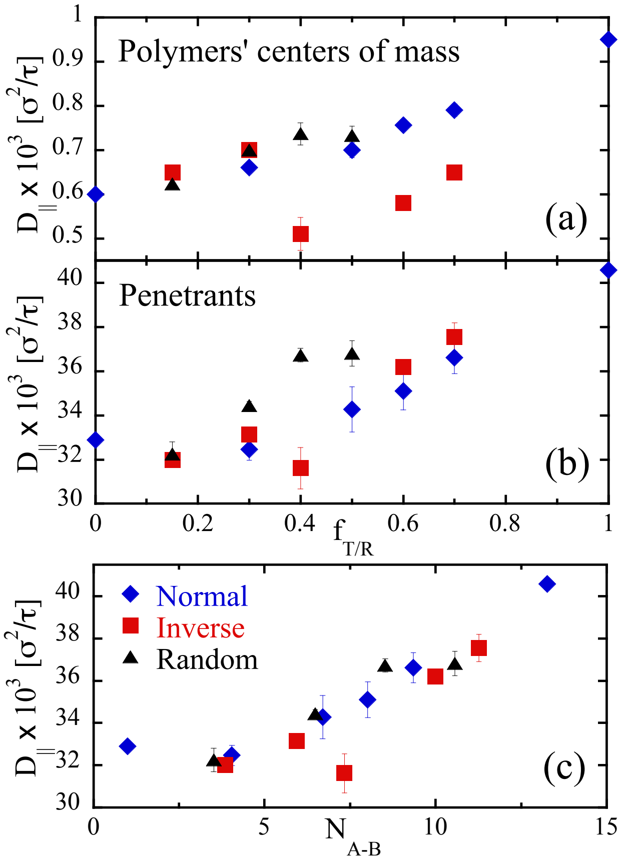

Figure 6. Anisotropic diffusion constants of (a) polymers' COM and (b) penetrants in parallel ($D_{||}$) directions (with respect to lamellar orientation) as a function of $f_{T/R}$ and (c) identical y-axis values as (b) but plotted against the average number of A-B bonds per chain. Error bars show the standard deviation across three independent runs and most are within the size of the points.

We calculate the anisotropic diffusion constants by fitting mean-squared displacements (MSD) data in the diffusive regime (Figure 6). For normal tapers and random midblocks, both polymers and penetrants generally diffuse faster in parallel directions as $f_{T/R}$ increases. Interestingly, polymers are only slightly faster in random midblocks than in normal TBPs, but penetrants show noticeably faster diffusion in random midblocks. Regardless of the midblock type, there is a monotonic increase of $D_{||}$ as there are more A-B bonds and interfaces become wider; the local A-B mixing boosts both polymers' and penetrants' parallel diffusion. The inverse TBPs show non-monotonic dynamic behavior for both polymers and penetrants. This is apparently the result of two competing factors: the local A-B mixing and chain conformations. Figure 6a shows the polymers' diffusion significantly drops at f_T = 0.4 where bridging conformations start to be significant.

To understand the impact of conformations, we report diffusion constants by conformation type. Each polymer is categorized by the conformation that it kept for the majority of the analyzed snapshots. We report the details including the number of polymers in each group and the frequency of their conformations in the Supporting Information. Briefly, we find that the polymers' $D_{||}$ is larger generally in the order of stretching-1 > folding > bridging > stretching-2 conformations, e.g. for 30% inverse TBPs, $D_{||} \times 10^3$ = 0.70$\pm$0.02 for stretching-1 and 0.69$\pm$0.02 for folding, and for 60% inverse TBPs, 0.59$\pm$0.02 for folding, 0.58$\pm$0.01 for bridging, and 0.45$\pm$0.06 for stretching-2 (units are σ^2/τ). It is intuitive that bridging and stretching-2 polymers are inherently slow because they are constrained by being linked at separate points to more than one lamellar layer. With increasing f_T > 0.4, the inverse TBPs show increasing parallel diffusion, due to the competitive interplay of increasing interfacial A-B mixing (which would ordinarily aid in diffusion) and sterically hindered chain conformations in these systems.

In Figure 6b, the *penetrants*' parallel diffusion in inverse TBPs shows a trend apparently more governed by the local A-B mixing effect rather than the conformation effect. Some long inverse tapers at f_T = 0.6, 0.7 even show higher penetrant diffusion than corresponding normal tapers, although their error bars overlap. This result is consistent with the comparison of parallel diffusion of polymers vs. penetrants in normal tapers and random midblocks. To further understand the local mixing effect on penetrants diffusion, we plotted the penetrant parallel diffusion constants against interfacial width and the number of A-B bonds. Figure 6c shows the plot versus the A-B bond numbers where almost all penetrants' diffusion constant values in the three different systems collapse on a curve (plotting versus interfacial width does not collapse the results – see the supporting information). This indicates that penetrants' diffusions are mostly governed by the local A-B mixing (represented by the number of A-B bonds) being less influenced by the conformation effect.

To summarize, we simulated uncharged-penetrant-doped normal and inverse TBPs, along with random midblock polymers. For normal tapers or random midblocks, polymers become less stretched and L_0 monotonically decreases with increasing $f_{T/R}$. In these systems, the increased interfacial A-B mixing leads to a monotonic increase of polymer and penetrant dynamics. However, the inverse tapered systems have non-monotonic trends in both structural and dynamic properties. We find this closely relates to the unique chain conformational behaviors (folding, bridging, or stretching across two lamella). Polymers of the latter two conformations are found to have slower parallel diffusion. Meanwhile, penetrants' parallel diffusion is not as strongly impacted—penetrant diffusion is more influenced by the local A-B mixing than the polymer conformations.

■ ASSOCIATED CONTENT

Supporting Information

Details of the simulation settings, additional data for structural and dynamic properties, and a comparison among three different potential models. Figures S1-S13, Tables S1, S2. This material is available free of charge via the Internet at http://pubs.acs.org.

■ AUTHOR INFORMATION

Corresponding Author

*E-mail: hall.1004@osu.edu.

Notes

The authors declare no competing financial interest.

■ ACKNOWLEDGMENTS

We thank Thomas Epps, III and Venkat Ganesan for helpful discussions and Jeffrey Ethier for help with additional calculations during the revision process. This material is based upon work supported by the

National Science Foundation under Grant No. 1454343 (L.M.H and Y.S). Additionally, this material is based upon work supported by the U.S. Department of Energy, Office of Science, Office of Basic Energy Sciences, under Award No. DE-SC0014209 (J.R.B.). We acknowledge the Ohio Supercomputer Center for providing compute resources.

■ REFERENCES

(1) Okamoto, K.; Fujii, M.; Okamyo, S.; Suzuki, H.; Tanaka, K.; Kita, H. Gas permeation properties of poly(ether imide) segmented copolymers. *Macromolecules* **1995**, *28*, 6950–6956.

(2) Lindner, S. M.; Hüttner, S.; Chiche, A.; Thelakkat, M.; Krausch, G. Charge separation at self-assembled nanostructured bulk interface in block copolymers. *Angew. Chemie - Int. Ed.* **2006**, *45*, 3364–3368.

(3) Elabd, Y. A.; Hickner, M. A. Block copolymers for fuel cells. *Macromolecules* **2011**, *44*, 1–11.

(4) Panday, A.; Mullin, S.; Gomez, E. D.; Wanakule, N.; Chen, V. L.; Hexemer, A.; Pople, J.; Balsara, N. P. Effect of molecular weight and salt concentration on conductivity of block copolymer elecrolytes. *Macromolecules* **2009**, *42*, 4632–4637.

(5) Cheng, S.; Smith, D. M.; Pan, Q.; Wang, S.; Li, C. Y. Anisotropic ion transport in nanostructured solid polymer electrolytes. *RSC Adv.* **2015**, *5*, 48793–48810.

(6) Singh, M.; Odusanya, O.; Wilmes, G. M.; Eitouni, H. B.; Gomez, E. D.; Patel, A. J.; Chen, V. L.; Park, M. J.; Fragouli, P.; Iatrou, H.; Hadjichristidis, N.; Cookson, D.; Balsara, N. P. Effect of molecular weight on the mechanical and electrical properties of block copolymer electrolytes. *Macromolecules* **2007**, *40*, 4578–4585.

(7) Gomez, E. D.; Panday, A.; Feng, E. H.; Chen, V.; Stone, G. M.; Minor, A. M.; Kisielowski, C.; Downing, K. H.; Borodin, O.; Smith, G. D.; Balsara, N. P. Effect of ion distribution on conductivity of block copolymer electrolytes. *Nano Lett.* **2009**, *9*, 1212–1216.

(8) Yuan, R.; Teran, A. A.; Gurevitch, I.; Mullin, S. A.; Wanakule, N. S.; Balsara, N. P. Ionic conductivity of low molecular weight block copolymer electrolytes. *Macromolecules* **2013**, *46*, 914–

921.

(9) Ganesan, V.; Pyramitsyn, V.; Bertoni, C.; Shah, M. Mechanisms underlying ion transport in lamellar block copolymer membranes. *ACS Macro Lett.* **2012**, *1*, 513–518.

(10) Kuan, W.-F.; Remy, R.; Mackay, M. E.; Epps, T. H. Controlled ionic conductivity via tapered block copolymer electrolytes. *RSC Adv.* **2015**, *5*, 12597–12604.

(11) Tsukahara, Y.; Nakamura, N.; Hashimoto, T.; Kawai, H. Structure and properties of tapered block polymers of styrene and isoprene. *Polym. J.* **1980**, *12*, 455–466.

(12) Hashimoto, T.; Tsukahara, Y.; Tachi, K.; Kawai, H. Structure and properties of tapered block polymers. 4. "Domain-boundary mixing" and "mixing-in-domain" effects on microdomain morphology and linear dynamic mechanical response. *Macromolecules* **1983**, *16*, 648–657.

(13) Hashimoto, T.; Tsukahara, Y.; Kawai, H. Structure and properties of tapered block polymers of styrene and isoprene II. Dynamic mechanical responses and their structural interpretations. *Polym. J.* **1983**, *15*, 699–711.

(14) Zielinski, J. M.; Spontak, R. J. Thermodynamic considerations of triblock copolymers with a random middle block. *Macromolecules* **1992**, *25*, 5957–5964.

(15) Pakula, T.; Matyjaszewski, K. Copolymers with controlled distribution of comonomers along the chain, 1. Structure, thermodynamics and dynamic properties of gradient copolymers. Computer simulation. *Macromol. Theory Simul.* **1996**, *5*, 987–1006.

(16) Hodrokoukes, P.; Floudas, G.; Pispas, S.; Hadjichristidis, N. Microphase separation in normal and inverse tapered block copolymers of polystyrene and polyisoprene. 1. Phase state. *Macromolecules* **2001**, *34*, 650–657.

(17) Harrats, C.; Fayt, R.; Jérôme, R. Effect of block copolymers of various molecular architecture on the phase morphology and tensile properties of LDPE rich (LDPE/PS) blends. *Polymer* **2002**, *43*, 863–873.

(18) Hodrokoukes, P.; Pispas, S.; Hadjichristidis, N. Controlling micellar properties of styrene/isoprene copolymers by altering the monomer arrangement along the chain. *Macromolecules* **2002**, *35*, 834–

840.

(19) Singh, N.; Tureau, M. S.; Epps, T. H. Manipulating ordering transitions in interfacially modified block copolymers. *Soft Matter* **2009**, *5*, 4757–4762.

(20) Huy, T. A.; Hai, L. H.; Adhikari, R.; Weidisch, R.; Michler, G. H.; Knoll, K. Influence of interfacial structure on morphology and deformation behavior of SBS block copolymers. *Polymer* **2003**, *44*, 1237–1245.

(21) Roy, R.; Park, J. K.; Young, W. S.; Mastroianni, S. E.; Tureau, M. S.; Epps, T. H. Double-gyroid network morphology in tapered diblock copolymers. *Macromolecules* **2011**, *44*, 3910–3915.

(22) Kuan, W.-F.; Roy, R.; Rong, L.; Hsiao, B. S.; Epps, T. H. Design and synthesis of network-forming triblock copolymers using tapered block interfaces. *ACS Macro Lett.* **2012**, *1*, 519–523.

(23) Brown, J. R.; Sides, S. W.; Hall, L. M. Phase behavior of tapered diblock copolymers from self-consistent field theory. *ACS Macro Lett.* **2013**, *2*, 1105–1109.

(24) Mastroianni, S. E.; Epps, T. H. Interfacial manipulations: controlling nanoscale assembly in bulk, thin film, and solution block copolymer systems. *Langmuir* **2013**, *29*, 3864–3878.

(25) Kuan, W.-F.; Reed, E. H.; Nguyen, N. A.; Mackay, M. E.; Epps, T. H. Using tapered interfaces to manipulate nanoscale morphologies in ion-doped block polymers. *MRS Commun.* **2015**, *5*, 251–256.

(26) Brown, J. R.; Seo, Y.; Maula, T. A. D.; Hall, L. M. Fluids density functional theory and initializing molecular dynamics simulations of block copolymers. *J. Chem. Phys.* **2016**, *144*, 124904.

(27) Seo, Y.; Brown, J. R.; Hall, L. M. Effect of tapering on morphology and interfacial behavior of diblock copolymers from molecular dynamics simulations. *Macromolecules* **2015**, *48*, 4974–4982.

(28) Levine, W. G.; Seo, Y.; Brown, J. R.; Hall, L. M. Effect of sequence dispersity on morphology of tapered diblock copolymers from molecular dynamics simulations. *J. Chem. Phys.* **2016**, *145*, 234907.

(29) Sethuraman, V.; Ganesan, V. Segmental dynamics in lamellar phases of tapered copolymers. *Soft Matter* **2016**, *12*, 7818–7823.

(30) Grest, G. S.; Lacasse, M.-D.; Kremer, K.; Gupta, A. M. Efficient continuum model for simulating polymer blends and copolymers. *J. Chem. Phys.* **1996**, *105*, 10583–10594.

(31) Ganesan, V.; Kumar, N. A.; Pryamitsyn, V. Blockiness and sequence polydispersity effects on the phase behavior and interfacial properties of gradient copolymers. *Macromolecules* **2012**, *45*, 6281–6297.

(32) Pandav, G.; Pryamitsyn, V.; Gallow, K. C.; Loo, Y.-L.; Genzer, J.; Ganesan, V. Phase behavior of gradient copolymer solutions: a Monte Carlo simulation study. *Soft Matter* **2012**, *8*, 6471–6482.

(33) Jiang, R.; Wang, Z.; Yin, Y.; Li, B.; Shi, A. C. Effects of compositional polydispersity on gradient copolymer melts. *J. Chem. Phys.* **2013**, *138*, 74906.

(34) Wang, Z.-G. Effects of ion solvation on the miscibility of binary polymer blends. *J. Phys. Chem. B* **2008**, *112*, 16205–16213.

(35) Qin, J.; de Pablo, J. J. Ordering transition in salt-doped diblock copolymers. *Macromolecules* **2016**, *49*, 3630–3638.

(36) Nakamura, I.; Balsara, N. P.; Wang, Z. G. First-order disordered-to-lamellar phase transition in lithium salt-doped block copolymers. *ACS Macro Lett.* **2013**, *2*, 478–481.

(37) Lytle, T. K.; Radhakrishna, M.; Sing, C. E. High charge density coacervate assembly via hybrid Monte Carlo single chain in mean field theory. *Macromolecules* **2016**, *49*, 9693–9705.

(38) Theodorou, D. N.; Suter, U. W. Shape of unperturbed linear polymers: polypropylene. *Macromolecules* **1985**, *18*, 1206–1214.

(39) Karayiannis, N. C.; Foteinopoulou, K.; Laso, M. The structure of random packings of freely jointed chains of tangent hard spheres. *J. Chem. Phys.* **2009**, *130*, 164908.

(40) Hall, L. M.; Seitz, M. E.; Winey, K. I.; Opper, K. L.; Wagener, K. B.; Stevens, M. J.; Frischknecht, A. L. Ionic aggregate structure in ionomer melts: effect of molecular architecture on aggregates and the ionomer peak. *J. Am. Chem. Soc.* **2012**, *134*, 574–587.

For Table of Contents Use Only

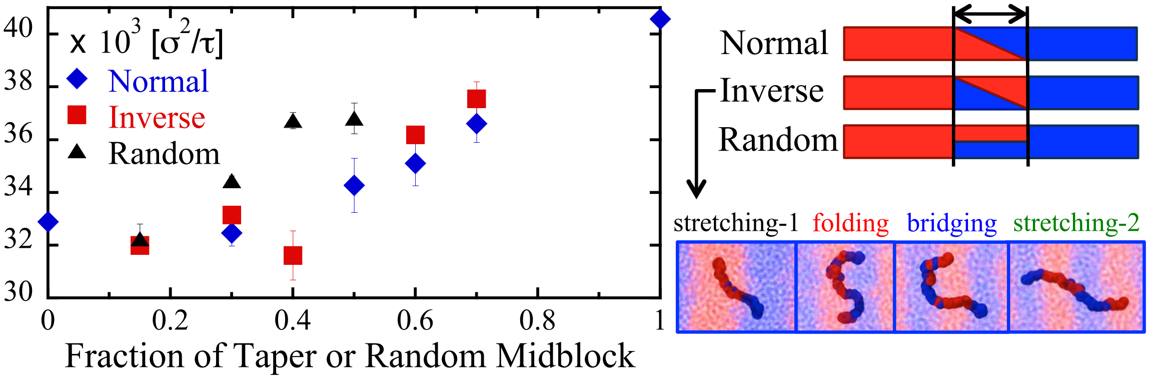Penetrants' diffusion constant parallel to lamellae